

# Compton Scattering from a High Pressure Polarized $^3\text{He}$ Target at HI $\gamma$ S

M.W. Ahmed<sup>1</sup>, C.W. Arnold<sup>2</sup>, T. Averett<sup>3</sup>, J.P. Chen<sup>4</sup> J.R.  
Calarco<sup>5</sup>, T. Clegg<sup>2</sup>, D. Dutta<sup>1</sup>, H. Gao<sup>1</sup> (Spokesperson),  
C. Howell<sup>1</sup>, M. Huang<sup>1</sup>, H. Karwowski<sup>2</sup>, G. Laskaris<sup>1</sup>, A. Nathan<sup>6</sup>,  
X. Qian<sup>1</sup>, H.R. Weller<sup>1</sup>, Y. Wu<sup>1</sup>, Q. Ye<sup>1</sup>, Q.J. Ye<sup>1</sup>, A. Young<sup>7</sup>, W.Z. Zheng<sup>1</sup>

<sup>1</sup>*Duke University*

<sup>2</sup>*University of North Carolina, Chapel Hill*

<sup>3</sup>*College of William & Mary*

<sup>4</sup>*Thomas Jefferson Lab National Accelerator Facility,  
Newport News, VA*

<sup>5</sup>*University of New Hampshire*

<sup>6</sup>*University of Illinois,  
Urbana-Champaign*

<sup>7</sup>*North Carolina State University, Raleigh*

## Abstract

The High Intensity Gamma Source (HI $\gamma$ S) at Duke Free Electron Laboratory opens new window to the study of fundamental quantities related to the structure of the nucleon through polarized Compton scattering from a polarized nuclear target. We propose first measurements of the spin-dependent asymmetries from elastic Compton scattering of circularly polarized photons on a high-pressure polarized  $^3\text{He}$  gas target. The proposed experiment will be carried out at a photon energy of 120 MeV. The Compton scattered photons will be detected by HI $\gamma$ S NaI Detector Array (HINDA) system. In combination with the forward and backward polarizabilities extracted from existing experiments, the proposed experiment will allow for the first time the extraction of all four neutron spin polarizabilities, and provide crucial tests of predictions based on effective field theories, dispersion theories, and lattice QCD calculations. We request a total beam time of 1260 hours with 100 % efficiency photon beam at a minimum photon flux of  $5 \times 10^7$ /sec for a photon energy spread of 3.0%.

## INTRODUCTION

Understanding the structure of the nucleon from the underlying theory of strong interaction in terms of quark and gluon degrees of freedom is a fundamental and challenging task in physics. The investigation of the nucleon structure experimentally and theoretically has been more than ever intense in the last two decades or so, largely due to progress and breakthrough achieved both in experiments and theories. With the development in polarized beam, recoil polarimetry, and polarized target technologies, polarization experiments have provided more precise data on quantities ranging from electromagnetic form factors of the nucleon from elastic electron-nucleon scattering to spin structure functions probed in deep inelastic lepton-nucleon scattering. At the same time, significant theoretical progress in areas ranging from effective field theories to lattice QCD calculations, has been made in describing these data and providing new insight in understanding the structure of the nucleon. The newly discovered Generalized Parton Distributions (GPDs) [1, 2], which can be accessed through deeply virtual Compton scattering and deeply virtual meson production, connect the nucleon form factors and the nucleon structure functions probed in the deep-inelastic scattering experiments. The GPDs provide new insights into the structure of the nucleon, and provide possibly a complete map of the nucleon wave-function.

Nucleon polarizabilities, comprise another set of fundamental quantities related to the structure of the nucleon, describing the response of the nucleon in external electromagnetic fields. These quantities can be accessed through low energy Compton scattering experiments. Compton scattering from nucleon at low energy is specified by low-energy theorems up to and including terms linear in photon energy. These terms are completely determined by the static properties of the nucleon, i.e. the nucleon charge, mass and its anomalous magnetic moment. Only at next to leading order in photon energy, there appear new structure constants which are related to the dynamic response of the nucleon internal degrees of freedom. The electric ( $\alpha$ ) and magnetic ( $\beta$ ) scalar polarizabilities, which describe the response of the nucleon to external electric and magnetic field, respectively, enter in terms which are second order in photon energy. At the third order, four new parameters,  $\gamma_1$  to  $\gamma_4$ , the spin polarizabilities appear. While spin polarizabilities do not have as intuitive a physical interpretation as the electric and magnetic polarizabilities, they are nevertheless just as fundamental. The close analogy in classical physics one can make to spin polarizabilities is the Faraday rotation in which the linear polarization of an incoming light is rotated going through a spin polarized medium.

Significant efforts have been devoted in the last two decades or so to Compton scattering measurements from proton in order to extract the proton electric ( $\alpha$ ) and magnetic ( $\beta$ ) polarizabilities. The most precise information on these two quantities are from the recent Mainz experiment [3]. A recent review [4] of the subject gives the following recommended experimental values:  $\alpha_p = 12.0 \pm 0.6$ ,  $\beta_p = 1.9 \mp 0.6$ , in units of  $10^{-4} \text{ fm}^3$ . While the proton electric and magnetic polarizabilities are known relatively well, our knowledge of the neutron polarizabilities is poorer than that of proton due to the lack of free neutron targets in nature. The neutron electric and magnetic polarizabilities have been extracted from experiments using nuclear targets: electromagnetic scattering of low-energy neutrons in the Coulomb field of heavy nuclei, coherent elastic Compton scattering by the deuteron, and the quasi-free Compton scattering from the deuteron. The most precise information on the neutron electric ( $\alpha_n$ ) and magnetic polarizabilities ( $\beta_n$ ) is from the quasifree Compton scattering experiment carried out at Mainz [5]. The recommended experimental values from

[4] are:  $\alpha_n = 12.5 \pm 1.7$ ,  $\beta_n = 2.7 \mp 1.8$ , in units of  $10^{-4} \text{ fm}^3$ .

Compared to the nucleon electric and magnetic polarizabilities, very little is known about nucleon spin polarizabilities. The only quantities which have been determined experimentally so far are the forward and backward spin polarizabilities,  $\gamma_0$  and  $\gamma_\pi$ . The forward and backward spin polarizabilities are two independent linear combinations of  $\gamma_1$ ,  $\gamma_2$  and  $\gamma_4$ . In order to determine all four spin polarizabilities separately, two additional measurements which are sensitive to the nucleon spin polarizabilities are needed. Unpolarized Compton scattering differential cross-section measurements are not sensitive to the nucleon spin polarizabilities. Double-polarization asymmetries from circularly polarized photons Compton scattering off a polarized nucleon target are expected to be sensitive to the nucleon spin polarizabilities. Such sensitivities have been demonstrated for the neutron by two independent calculations [6, 7]. Recently, double polarized asymmetry with linearly polarized photons have been shown [8] to be sensitive to proton spin polarizabilities in the energy range between the pion production threshold and the  $\Delta(1232)$  resonance. Recently, double polarized elastic Compton scattering on  $^3\text{He}$  has been investigated [9] and sensitivities to neutron spin polarizabilities have been shown.

We propose a double-polarization compton scattering experiment in which circularly polarized photons scattering off a polarized  $^3\text{He}$  target. A polarized  $^3\text{He}$  target is an effective polarized neutron target because of its unique ground state spin structure in which the spins of the two proton pairs off and the unpaired neutron carries to first order the  $^3\text{He}$  spin. Spin-dependent asymmetries at elastic kinematics will be measured with target spin direction being parallel and perpendicular to the incident photon momentum direction in the scattering plane, respectively. These spin-dependent asymmetries are sensitive to the neutron spin polarizabilities [6, 7, 9].

The rest of the proposal is organized as following. Section II contains the formulism for spin-dependent compton scattering. Section III discusses predictions on spin polarizabilities from chiral effective field theory and the dispersion analysis. Section IV contains detailed description of the proposed experiment and the projected sensitivities to the neutron spin polarizabilities. Lastly, Section V discusses the responsibilities of the collaboration in carrying out such an experiment.

## COMPTON SCATTERING AT LOW ENERGIES

The general amplitude for Compton scattering based on parity, charge conjugation, and time reversal symmetry can be written in terms of six structure dependent functions  $A_i(\omega, \theta)$ ,  $i = 1, \dots, 6$  as:

$$\begin{aligned}
T = & A_1(\omega, \theta) \vec{\epsilon}^{\prime*} \cdot \vec{\epsilon} + A_2(\omega, \theta) \vec{\epsilon}^{\prime*} \cdot \hat{k} \vec{\epsilon} \cdot \hat{k}' \\
& + iA_3(\omega, \theta) \vec{\sigma} \cdot (\vec{\epsilon}^{\prime*} \times \vec{\epsilon}) + iA_4(\omega, \theta) \vec{\sigma} \cdot (\hat{k}' \times \hat{k}) \vec{\epsilon}^{\prime*} \cdot \vec{\epsilon} + \\
& iA_5(\omega, \theta) \vec{\sigma} \cdot \left[ (\vec{\epsilon}^{\prime*} \times \hat{k}) \vec{\epsilon} \cdot \hat{k}' - \vec{\epsilon} \times \hat{k}' \vec{\epsilon}^{\prime*} \cdot \hat{k} \right] \\
& iA_6(\omega, \theta) \vec{\sigma} \cdot \left[ (\vec{\epsilon}^{\prime*} \times \hat{k}') \vec{\epsilon} \cdot \hat{k} - \vec{\epsilon} \times \hat{k} \vec{\epsilon}^{\prime*} \cdot \hat{k}' \right],
\end{aligned} \tag{1}$$

where  $\omega = \omega'$  denoting the photon energy in the center-of-mass frame,  $\theta$  is the center-of-mass scattering angle of the photon,  $\vec{\epsilon}, \hat{k}$  ( $\vec{\epsilon}', \hat{k}'$ ) are the polarization vector and direction of

the incident (final) photon, and  $\sigma$  represents the spin (polarization) vector of the nucleon. Following the general conventions, the six structure dependent functions,  $A_i(\omega, \theta)$  ( $i = 1, \dots, 6$ ) are separated into the pion-pole (“anomalous”) contributions and the remaining (“regular”) terms:

$$A_i(\omega, \theta) = A_i(\omega, \theta)^{\pi^0\text{-pole}} + A_i(\omega, \theta)^{\text{reg}} \quad (2)$$

One can now carry out a low energy expansion of the six “regular” structure functions in powers of photon energy.

$$A_1(\omega, \theta)_{c.m.}^{\text{reg}} = -Q \frac{e^2}{M_N} + 4\pi(\alpha_E + \cos\theta\beta_M)\omega^2 + \frac{4\pi}{M_N}(\alpha_E + \beta_M)(1 + \cos\theta)\omega^3 + O(\omega^4, \frac{1}{M_N^3}), \quad (3)$$

$$A_2(\omega, \theta)_{c.m.}^{\text{reg}} = Q \frac{e^2}{M_N^2}\omega - 4\pi\beta_M\omega^2 - \frac{4\pi}{M_N}(\alpha_E + \beta_M)\omega^3 + O(\omega^4, \frac{1}{M_N^3}), \quad (4)$$

$$A_3(\omega, \theta)_{c.m.}^{\text{reg}} = [Q(Q + 2\kappa) - (Q + \kappa)^2 \cos\theta] \frac{e^2}{2M_N^2}\omega + 4\pi[\gamma_1 - (\gamma_2 + 2\gamma_4) \cos\theta]\omega^3 + O(\omega^4, \frac{1}{M_N^3}), \quad (5)$$

$$A_4(\omega, \theta)_{c.m.}^{\text{reg}} = -\frac{(Q + \kappa)^2 e^2}{2M_N^2}\omega + 4\pi\gamma_2\omega^3 + O(\omega^4, \frac{1}{M_N^3}), \quad (6)$$

$$A_5(\omega, \theta)_{c.m.}^{\text{reg}} = \frac{(Q + \kappa)^2 e^2}{2M_N^2}\omega + 4\pi\gamma_4\omega^3 + O(\omega^4, \frac{1}{M_N^3}), \quad (7)$$

$$A_6(\omega, \theta)_{c.m.}^{\text{reg}} = -\frac{Q(Q + \kappa)e^2}{2M_N^2}\omega + 4\pi\gamma_3\omega^3 + O(\omega^4, \frac{1}{M_N^3}), \quad (8)$$

where the charge of the nucleon is  $Q = (1 + \tau_3)/2$ , its anomalous magnetic moment is  $\kappa = (\kappa_s + \kappa_v\tau_3)/2$ , and the mass of the nucleon is  $M_N$ . For each structure function the leading order terms in the  $\omega$  expansion are given by *model-independent* Born contributions for scattering from a spin 1/2 point particle with anomalous magnetic moment and are fixed by low energy theorems of current algebra. The higher order terms in  $\omega$  are model dependent quantities and the comparison between data and theoretical predictions provides sensitive tests of the validity of the theoretical approaches. The more familiar electric ( $\alpha_E$ ) and magnetic ( $\beta_M$ ) polarizabilities enter the amplitude at the  $O(\omega^2)$  and measure the response or deformation of the system in quasi-static electric and magnetic fields. The  $\gamma_i$  ( $i = 1, \dots, 4$ ), which enters the amplitude at the  $\omega^3$  order are the so-called *spin polarizabilities*. They determine independently the response of a microscopic target with spin 1/2 to quasi-static electromagnetic field when the spin degree of freedom is involved. For example, an induced dipole  $\vec{p}_s$  can be constructed by  $\vec{p}_s = \gamma_3 \vec{\Delta}(\vec{S} \cdot \vec{B})$ , where  $\vec{S}$  denotes the spin of the target.

The forward and backward spin polarizabilities ( $\gamma_0$  and  $\gamma_\pi$ ) are linear combination of  $\gamma_i$ :

$$\gamma_0 = \gamma_1 - \gamma_2 - 2\gamma_4 \quad (9)$$

$$\gamma_\pi = \gamma_1 + \gamma_2 + 2\gamma_4$$

Both  $\gamma_0$  and  $\gamma_\pi$  can be obtained in model dependent way relying on multiple analysis of single pion photoproduction data.

Recently, the backward spin polarizability  $\gamma_\pi = \gamma_1 + \gamma_2 + 2\gamma_4$  has been extracted by the LEGS group for the first time from unpolarized Compton scattering data from the proton [10]. However, the extracted value  $\gamma_\pi = (-27.1 \pm 2.2) \times 10^{-4} \text{ fm}^4$  contradicts with predictions of standard dispersion theory [11–13] and also with chiral perturbation theory [14–16]. The theoretical prediction for  $\gamma_\pi$  from chiral effective field theory is  $-36.7 \times 10^{-4} \text{ fm}^4$  [14]. The LEGS result is also in disagreement with the TAPS result  $\gamma_\pi = (-36.1 \pm 2.2) \times 10^{-4} \text{ fm}^4$  [3]. The most recent Mainz experiment [17] using the LARA detector, extracted a backward polarizability value ranging from  $(-35.9 \text{ to } -40.9) \times 10^{-4} \text{ fm}^4$  depending on the parameterization used for the photomeson amplitudes, which is in agreement with the earlier result from Mainz [3]. The new data confirm the previous observation that there is a systematic discrepancy between Mainz results and LEGS' results. The clarification of the situation will benefit from double polarization Compton scattering experiments [18] in which circularly polarized photons scattering off a polarized proton target. The recommended experimental value from [4] is  $\gamma_\pi^p = (-38.7 \pm 1.8) \times 10^{-4} \text{ fm}^4$ . The neutron backward spin polarizability was determined to be  $\gamma_\pi^n = (58.6 \pm 4.0) \times 10^{-4} \text{ fm}^4$  [4, 19].

A sum rule exists for  $\gamma_0$ , which was originally discovered by Gell-Mann, Goldberger and Thirring (GGT) [20]:

$$\gamma_0 = \frac{1}{4\pi^2} \int_{\nu_0}^{\infty} \frac{d\omega}{\omega^3} [\sigma_-(\omega) - \sigma_+(\omega)], \quad (10)$$

where  $\nu_0$  is the pion production threshold, and  $\sigma_-(\omega)$ ,  $\sigma_+(\omega)$  are the total photoabsorption cross-section for the total helicity of the photon-nucleon system to be  $1/2$  and  $3/2$  along the photon momentum direction, respectively. The GGT sum rule is closely related to the Drell-Hearn-Gerasimov (DHG) sum rule [21], which has renewed enormous interest in recent years both experimentally and theoretically.

$$\frac{\pi e^2 \kappa^2}{2M_N^2} = - \int_{\nu_0}^{\infty} \frac{d\omega}{\omega} [\sigma_-(\omega) - \sigma_+(\omega)]. \quad (11)$$

The following results on  $\gamma_0$  were estimated using the VPI-FA93 multipole analysis [22]:

$$\begin{aligned} \gamma_0 &\sim -1.34 \times 10^{-4} \text{ fm}^4 \text{ (proton)} \\ \gamma_0 &\sim -0.38 \times 10^{-4} \text{ fm}^4 \text{ (neutron)} \end{aligned} \quad (12)$$

The most recent extraction of the proton forward spin polarizability is from the Mainz GDH experiment [23], and the extracted value of  $\gamma_0$  based on the Mainz GDH data and the dispersion analysis is  $\gamma_0 = [-1.01 \pm 0.08(\text{stat}) \pm 0.10(\text{syst})] \times 10^{-4} \text{ fm}^4$  [24].

Dynamical dipole polarizabilities are also commonly used in the literature. Following the formalism of [7], one obtains the following by carrying out a multipole expansion for  $l = 1$  for nucleon Compton scattering in the center-of-mass frame in terms of dynamical polarizabilities:

$$\bar{A}_1(\omega, z) = \frac{4\pi W}{M_N} [\alpha_{E1}(\omega) + z\beta_{M1}(\omega)\omega^2] + O(l = 2) \quad (13)$$

$$\bar{A}_2(\omega, z) = -\frac{4\pi W}{M_N} \beta_{M1(\omega)} \omega^2 + O(l=2), \quad (14)$$

$$\bar{A}_3(\omega, z) = -\frac{4\pi W}{M_N} [\gamma_{E1E1}(\omega) + z\gamma_{M1M1}(\omega) + \gamma_{E1M2}(\omega) + z\gamma_{M1E2}(\omega)] \omega^3 + O(l=2), \quad (15)$$

$$\bar{A}_4(\omega, z) = \frac{4\pi W}{M_N} [-\gamma_{M1M1}(\omega) + \gamma_{M1E2}(\omega)] \omega^3 + O(l=2), \quad (16)$$

$$\bar{A}_5(\omega, z) = \frac{4\pi W}{M_N} \gamma_{M1M1}(\omega) \omega^3 + O(l=2), \quad (17)$$

$$\bar{A}_6(\omega, z) = \frac{4\pi W}{M_N} \gamma_{E1M2}(\omega) \omega^3 + O(l=2), \quad (18)$$

where  $W = \sqrt{s}$  is the total center-of-mass energy, and  $z = \cos(\theta)$  with  $\theta$  being the center-of-mass scattering angle. The four spin polarizabilities,  $\gamma_{E1E1}$ ,  $\gamma_{M1M1}$ ,  $\gamma_{E1M2}$ ,  $\gamma_{M1E2}$ , relate to a multipole expansion describing the nucleon spin response at the third order. For example,  $\gamma_{E1M2}$  corresponds to the excitation of the nucleon by a magnetic quadrupole field ( $M2$ ) and its de-excitation by an electric dipole ( $E1$ ) field. The forward and the backward spin polarizabilities,  $\gamma_0$  and  $\gamma_\pi$  can be written in terms of the linear combination of these four spin polarizabilities:

$$\gamma_0 = -\gamma_{E1E1} - \gamma_{M1M1} - \gamma_{E1M2} - \gamma_{M1E2} \quad (19)$$

$$\gamma_\pi = -\gamma_{E1E1} + \gamma_{M1M1} - \gamma_{E1M2} + \gamma_{M1E2} \quad (20)$$

## CALCULATIONS OF NUCLEON SPIN POLARIZABILITIES

### Effective field theory calculations

Recently, calculations of the nucleon spin polarizabilities have been carried out at next-to-leading order (NLO) in chiral perturbation theory by several groups [15, 16, 25]. Kumar, McGovern and Birse [16] calculated all four spin polarizabilities at NLO in heavy-baryon chiral perturbation theory and obtained the following results:

$$\begin{aligned} \gamma_1 &= [-21.3]\tau_3 + 4.5 - (2.1 + 1.3\tau_3) \\ \gamma_2 &= 2.3 - (3.1 + 0.7\tau_3) \\ \gamma_3 &= [10.7]\tau_3 + 1.1 - (0.8 + 0.1\tau_3) \\ \gamma_4 &= [-10.7]\tau_3 - 1.1 + (3.9 + 0.5\tau_3) \\ \gamma_0 &= 4.5 - (6.9 + 1.5\tau_3) \\ \gamma_\pi &= [-42.7]\tau_3 + 4.5 + (2.7 - 1.1\tau_3), \end{aligned} \quad (21)$$

where term in square brackets is the third-order pion pole (anomalous) contribution, where it exists. The forward spin polarizability obtained is in good agreement with that

calculated by Ji, Kao and Osborne [25]. These results are also consistent with results obtained by Gellas, Hemmert and Meissner [15] once difference in the definition of the spin polarizabilities is accounted for [26]. However, the prediction for  $\gamma_0$  is in disagreement with the most recent  $\gamma_0$  result extracted from Mainz experiment [24].

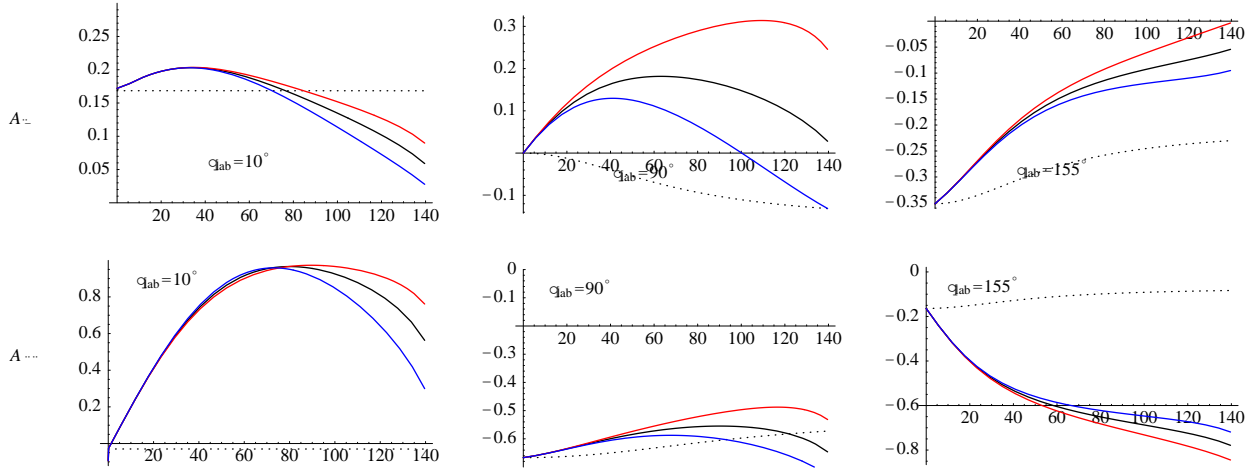
As described previously, the forward and the backward spin polarizabilities can be extracted in a model dependent way via multipole analysis of the unpolarized single pion photoproduction data. However, there are systematic differences between the Mainz results and the LEGS' on  $\gamma_\pi$  at the present time. Compton scattering with double polarizations are sensitive to individual spin polarizabilities, which will provide more stringent test of the theory and shed light on the discrepancy between the Mainz data and the LEGS' on  $\gamma_\pi$ .

### Double Polarization Asymmetry from Compton Scattering on a nucleon

Spin polarizabilities of the nucleon can be probed directly via circularly polarized photons Compton scattering off from a polarized nucleon target. Fig. 1 shows the sensitivity of double polarization asymmetry to neutron spin polarizability  $\gamma_1$  as a function of photon energy in the lab and for various photon scattering angles in the lab. The photon is always circularly polarized, and  $A_\perp$  and  $A_\parallel$  corresponds to the target spin being perpendicular and parallel to the incident photon momentum direction in the reaction plane, respectively. The black curve is the asymmetry predicted from a fourth-order chiral perturbation theory [6, 16], and the red (blue) curve corresponds to varying  $\gamma_1$  by  $-10\%$  ( $+10\%$ ), leaving all other polarizability values fixed. The black dotted curve is the Born term only which includes the pion pole contribution. Fig. 2 is the corresponding asymmetry results showing sensitivity to neutron  $\gamma_2$ , and Fig. 3 and Fig. 4 are similar results showing sensitivity to neutron  $\gamma_3$  and  $\gamma_4$ , respectively. All the calculations are carried out for a free polarized "neutron" target, and the neutron electric and magnetic polarizability values of  $\alpha = 12, \beta = 2$  are used in all these calculations. Fig. 5 shows the sensitivity of the double polarization asymmetries to the neutron electric and magnetic polarizabilities. The red curve corresponds to  $\alpha = 10, \beta = 4$ , and the blue curve is for  $\alpha = 8, \beta = 6$ .

These results show that the perpendicular asymmetry  $A_\perp$  is most sensitive to the neutron spin polarizabilities  $\gamma_1$  and  $\gamma_2$  at a photon scattering angle of  $90^\circ$  in the lab frame. The parallel asymmetry  $A_\parallel$  is sensitive to the neutron spin polarizability  $\gamma_1, \gamma_2, \gamma_4$  at a photon scattering angle of  $10^\circ$  when the incident photon energy is relatively large,  $\geq 100$  MeV. While sensitivity to neutron  $\alpha, \beta$  is shown in Fig. 5, these spin-dependent asymmetries are much more sensitive to the unknown neutron spin polarizabilities  $\gamma_i$ . Therefore, the spin-dependent Compton scattering of circularly polarized photons from a polarized "neutron" target will allow sensitive probe of the neutron spin polarizabilities. The corresponding results for proton are shown in Fig. 6-Fig. 9. One sees clearly that these double polarization asymmetries are more sensitive to spin polarizabilities in the case of neutron than that of proton. This is because the Born contribution dominates the Compton scattering in the case of the proton.

Since there is no free neutron target in nature, effective neutron target, i.e. nuclear targets, deuteron and  $^3\text{He}$  nucleus are commonly used for the study of the neutron. A polarized  $^3\text{He}$  nucleus is very useful in probing the neutron electromagnetic and spin structure because of the unique spin structure of the  $^3\text{He}$  ground state. It is dominated by a spatially symmetric  $S$  wave in which the proton spins pair off and the spin of the  $^3\text{He}$  nucleus is carried by the unpaired neutron [27, 28].



W lab

FIG. 1: Compton scattering double polarization asymmetry as a function of photon energy in MeV for different photon scattering angle in the lab. The sensitivity to neutron spin polarizability  $\gamma_1$  is shown by the difference between red (blue) curve and the black curve (see text for details). The upper panel is the  $A_{\perp}$ , and the lower panel is the  $A_{\parallel}$ .

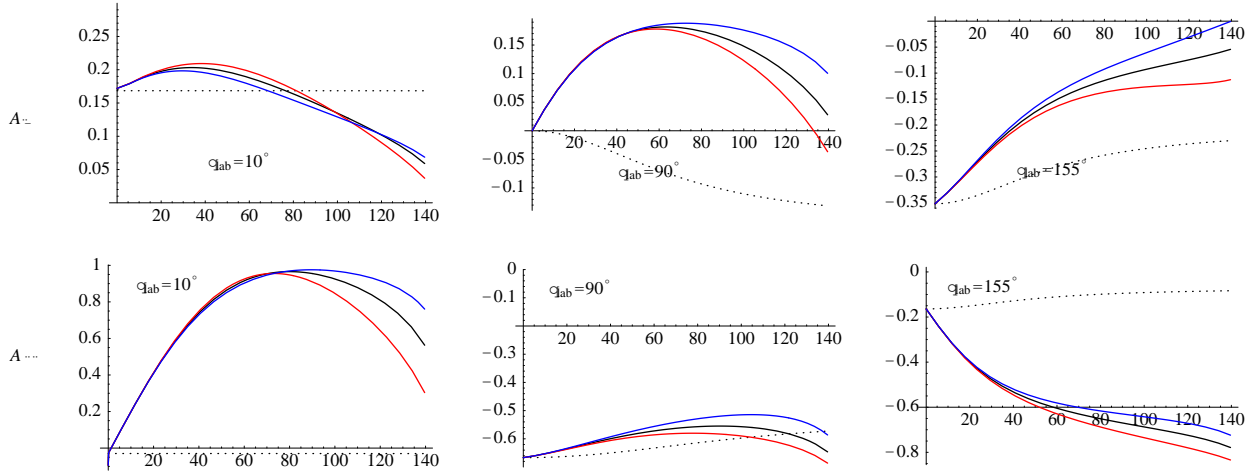
### Double Polarization Asymmetry from Compton Scattering on a polarized ${}^3\text{He}$

One can also extract the neutron spin polarizabilities from polarized Compton scattering from a polarized  ${}^3\text{He}$  target at the elastic kinematics as demonstrated by a recent next-to-leading order chiral perturbation theory calculation [9]. Further, the calculation shows [29] that sensitivities to the proton spin polarizabilities are highly suppressed in the double-polarization observables. The amplitude for Compton scattering from polarized  ${}^3\text{He}$  is a sum of one-body and two-body parts.

$$T_{\gamma^3\text{He}} = \sum_{i=1\dots 6} A_i^{3\text{He}} t_i,$$

$$A_i^{3\text{He}} = A_i^{1B} + A_i^{2B}.$$

Here,  $t_i$  are invariants constructed out of the photon momentum and polarization vectors.  $A_i^{1B}$  ( $A_i^{2B}$ ) are one-body and two-body Compton structure functions. Calculation [29] shows that  $A_i^{2B}$ ,  $i = 1\dots 6$  are negligible at  $\mathcal{O}(Q^3)$ . Moreover, in a polarized  ${}^3\text{He}$  target spin of the two protons are treated anti-aligned, therefore the neutron carries the major contribution to the nuclear spin. Hence, we expect that  $A_i^{3\text{He}} \approx A_i^n$ , which supports the idea than Compton scattering on  ${}^3\text{He}$  is an ideal avenue to extract neutron polarizabilities. Experimentally, one



W lab

FIG. 2: Compton scattering double polarization asymmetry as a function of photon energy in MeV for different photon scattering angle in the lab. The sensitivity to neutron spin polarizability  $\gamma_2$  is shown by the difference between red (blue) curve and the black curve (see text for details). The upper panel is the  $A_{\perp}$ , and the lower panel is the  $A_{\parallel}$ .

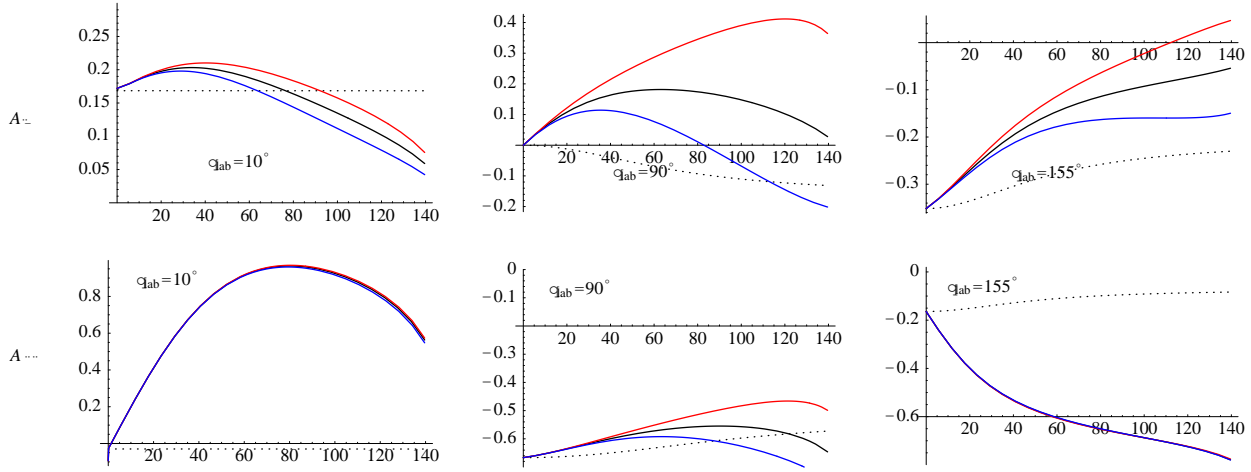
has to suppress backgrounds during the experiment using the FEL beam RF structure as demonstrated successfully in the  $^{16}\text{O}$  Compton scattering experiment [30] at HI $\gamma$ S. Fig. 10 shows the differential cross-section (DCS) calculated by Choudhury *et al.* [9] for elastic Compton scattering from  $^3\text{He}$  as a function of the scattered photon angle for an incident photon energy of 100 MeV (120 MeV) in the left (right) panel in the center-of-mass frame. In Fig. 10, the red curve is the result at the next-to-leading order, but without the two-body contribution. The blue curve is the result at the the next-to-lead order with two-body contribution. The green curve is the calculation including the proton Thomson term only. For details, see Ref. [9]. Fig. 11 shows the calculated sensitivities of the unpolarized DCS to  $\alpha_n$  (left) and  $\beta_n$  (right) for incident photon energy of 100 MeV (120 MeV) in the upper (lower) panel.

The spin dependent differential cross section difference  $\Delta_z$  and  $\Delta_x$  are defined as following:

$$\Delta_z = \frac{d\sigma}{d\Omega_{\uparrow\uparrow}} - \frac{d\sigma}{d\Omega_{\uparrow\downarrow}} \quad (22)$$

$$\Delta_x = \frac{d\sigma}{d\Omega_{\uparrow\rightarrow}} - \frac{d\sigma}{d\Omega_{\uparrow\leftarrow}},$$

where  $z$  ( $x$ ) refers to the target spin along the incident photon momentum direction



W lab

FIG. 3: Compton scattering double polarization asymmetry as a function of photon energy in MeV for different photon scattering angle in the lab. The sensitivity to neutron spin polarizability  $\gamma_3$  is shown by the difference between red (blue) curve and the black curve (see text for details). The upper panel is the  $A_{\perp}$ , and the lower panel is the  $A_{\parallel}$ .

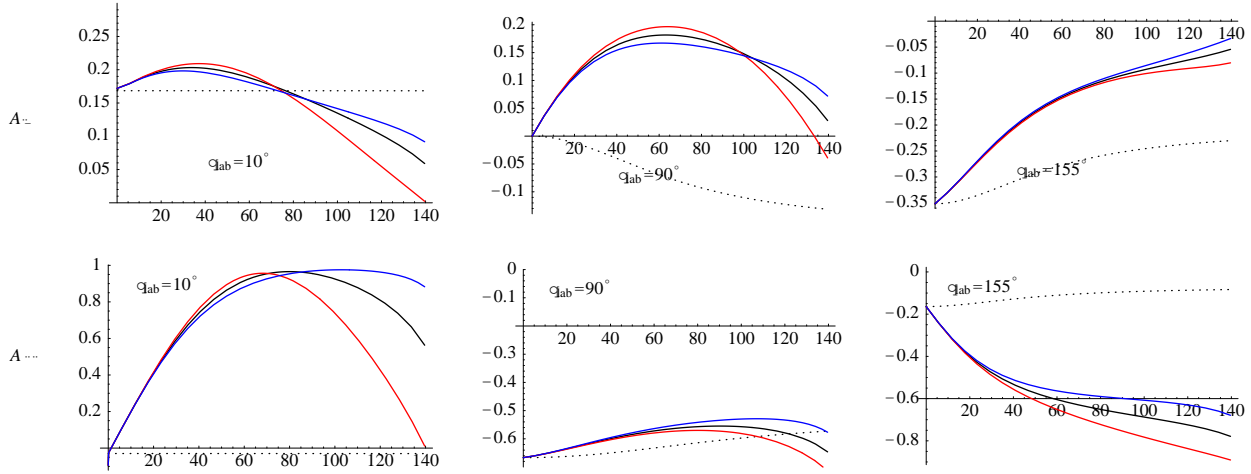
(transverse to it) in the scattering plane. The photons are always circularly polarized. The corresponding spin dependent asymmetries are defined as:

$$A_z = \frac{\frac{d\sigma}{d\Omega}_{\uparrow\uparrow} - \frac{d\sigma}{d\Omega}_{\uparrow\downarrow}}{\frac{d\sigma}{d\Omega}_{\uparrow\uparrow} + \frac{d\sigma}{d\Omega}_{\uparrow\downarrow}} \quad (23)$$

$$A_x = \frac{\frac{d\sigma}{d\Omega}_{\uparrow\rightarrow} - \frac{d\sigma}{d\Omega}_{\uparrow\leftarrow}}{\frac{d\sigma}{d\Omega}_{\uparrow\rightarrow} + \frac{d\sigma}{d\Omega}_{\uparrow\leftarrow}},$$

Fig. 12 shows the sensitivities of  $\Delta_z$  to the neutron spin polarizabilities,  $\gamma_i$  ( $i = 1 - 4$ ) (in the order from left to right and top to bottom) by varying the corresponding spin polarizabilities. Fig. 13 is the corresponding plot for  $\Delta_x$ . These calculations are for photon energy  $\omega = 120$  MeV. While  $\Delta_z$  is most sensitive to  $\gamma_1$ ,  $\gamma_2$  and  $\gamma_4$  at forward Compton scattering angles,  $\Delta_x$  is most sensitive to  $\gamma_1$  at angles between 100-120 degrees, and to  $\gamma_4$  over a relatively large angle range. Fig. 14 (Fig. 15) shows the corresponding sensitivities of  $A_z$  ( $A_x$ ) to the neutron spin polarizabilities  $\gamma_i$  ( $i = 1 - 4$ ).

Since there is no free neutron target, one should carry out the double polarized Compton scattering from a polarized  $^3\text{He}$  target to form  $\Delta_z$  ( $\Delta_x$ ) and  $A_z$  ( $A_x$ ). These measurements



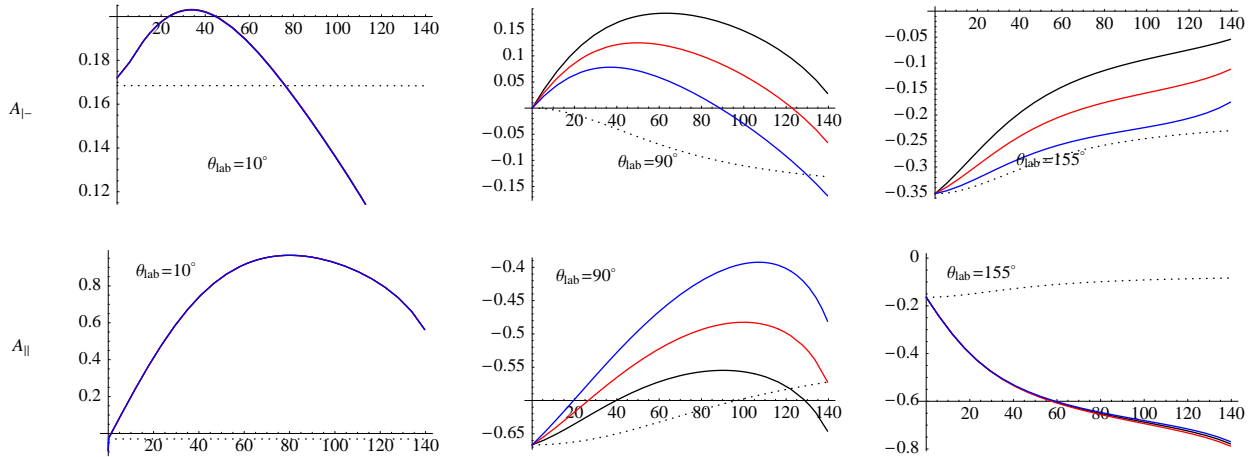
W lab

FIG. 4: Compton scattering double polarization asymmetry as a function of photon energy in MeV for different photon scattering angle in the lab. The sensitivity to neutron spin polarizability  $\gamma_4$  is shown by the difference between red (blue) curve and the black curve (see text for details). The upper panel is the  $A_{\perp}$ , and the lower panel is the  $A_{\parallel}$ .

allow the extraction of two combination of the neutron spin polarizabilities  $\gamma_i (i = 1 - 4)$ . Moreover, from  $\gamma d$  scattering data [29], we can extract the combination of  $\gamma_1$  and  $\gamma_3$ . If combining all the information, we can at least extract two spin polarizabilities and provide constrain on the other two. Consider the neutron polarizabilities sensitivity of the photon energy, we plan to carry out the polarized elastic Compton scattering experiment at HI $\gamma$ S with 120 MeV photon energy (under  $\pi$  production).

## THE EXPERIMENTAL OVERVIEW

We propose a double polarization compton scattering experiment of circularly polarized photons from a polarized  $^3\text{He}$  nuclear target at the elastic kinematics using the High Intensity Gamma Source (HI $\gamma$ S) at the Duke Free Electron Laser Lab. The scattered photons will be detected by using HI $\gamma$ S NaI Detector Array (HINDA) system. The 2% energy resolution of the NaI detector is sufficient for separating the elastic process from the quasifree processes. The polarized  $^3\text{He}$  target is a high-pressure target based on the spin-exchange optical pumping technique. The double polarization asymmetry will be formed by flipping the circular polarization of the incident photon beam. The target spin direction will be reversed from time to time to minimize effects due to systematic false asymmetries. Based on predictions



$\omega_{\text{lab}}$

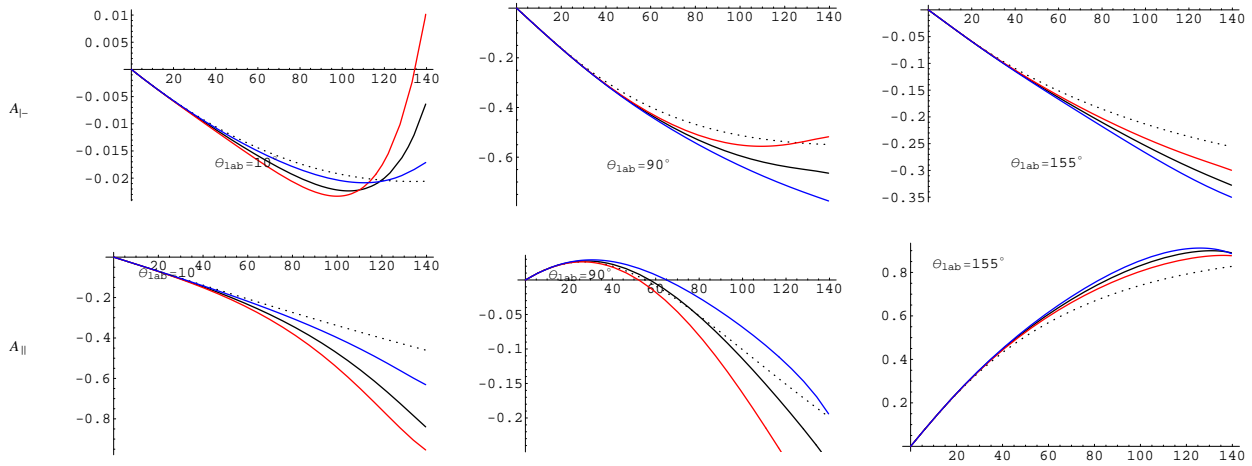
FIG. 5: Compton scattering double polarization asymmetry as a function of photon energy for different photon scattering angle in the lab. The sensitivity to neutron electric and magnetic polarizability  $\alpha, \beta$  is shown by the difference between red (blue) curve and the black curve (see text for details). The upper panel is the  $A_{\perp}$ , and the lower panel is the  $A_{\parallel}$ .

from Choudhury *et al.* [9], the aforementioned quantities are most sensitive to neutron spin polarizabilities when the  $^3\text{He}$  target is polarized along the incident photon momentum,  $z$  direction. In this experiment, we will align the target spin parallel or anti-parallel to the incident photon momentum direction in the scattering plane to measure the longitudinal asymmetry ( $A_{\parallel}$ ) and helicity-dependent differential cross section ( $\Delta_z$ ). The photon energy of the proposed experiment is 120 MeV. The details of the experiment will be discussed in the next section.

## THE EXPERIMENT

### The HI $\gamma$ S Facility

The HI $\gamma$ S facility at Duke FEL is based on the Compton backscattering of intracavity UV-FEL light from electrons circulating in a storage ring. The advantage of such a scheme compared to Compton backscattering of conventional laser light is the enhancement of a  $\gamma$ -flux by approximately three orders of magnitude over the existing sources. The Duke storage ring was designed to operate at energies from 250 MeV to 1 GeV. The range of operating energies has been extended to between 200 MeV and 1.1 GeV as demonstrated in 1995.



$\omega_{\text{lab}}$

FIG. 6: Compton scattering double polarization asymmetry as a function of photon energy for different photon scattering angle in the lab. The sensitivity to proton spin polarizability  $\gamma_1$  is shown by the difference between red (blue) curve and the black curve (see text for details).

The Duke OK-4 storage ring XUV FEL can presently produce FEL photons up to 12.5 eV, which will allow the production of  $\gamma$  rays up to an energy of about 225 MeV having an average flux in excess of  $10^7$  /sec/MeV. This can be obtained with a modest beam of 100 mA in a lasing bunch and 10 mA in a target bunch. If necessary, the flux of  $\gamma$  rays can be increased by increasing the current in the target bunch, increasing the current in the lasing bunch, and/or by operating four electron bunches (two lasing bunches and two target bunches). The storage ring is limited to average currents of 1 A. Within these constraints, the maximum  $\gamma$ -ray output is  $3 \times 10^8$  photons/sec/MeV.

The energy of the  $\gamma$  rays transmitted by the collimator will be almost entirely at the kinematic's upper limit. Thus, the degree of polarization of the  $\gamma$  rays will very nearly (within 1%) equal to that of the FEL photons (100%). In the basic configuration the FEL photons are polarized linearly in the horizontal plane. In this experiment, circularly polarized photons are needed for the proposed measurements. Furthermore, the helicity of the  $\gamma$  rays needs to be flipped rapidly (on the order of a second) in order to form the spin-dependent asymmetry from Compton scattering. Obtaining arbitrary, switchable polarization will be achieved by the insertion of birefringent cells in front of each mirror in the lasing cavity. To obtain circularly polarized  $\gamma$  rays, each cell will be set to produce a  $\lambda/8$  plate. FEL photons initially polarized horizontally in the wiggler will encounter a  $\lambda/8$  plate, be reflected, and again pass through the same  $\lambda/8$  plate. The combined effect will be that of a  $\lambda/4$  plate so

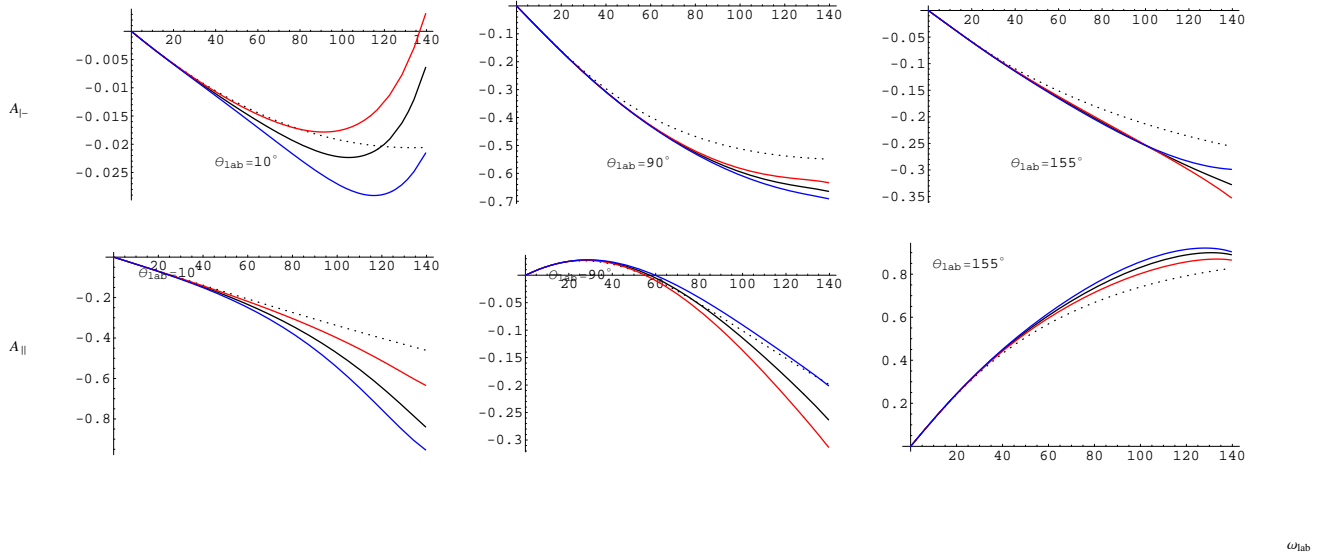


FIG. 7: Compton scattering double polarization asymmetry as a function of photon energy for different photon scattering angle in the lab. The sensitivity to proton spin polarizability  $\gamma_2$  is shown by the difference between red (blue) curve and the black curve (see text for details).

the photons will have circular polarization when they intersect the scattering bunch. The  $\gamma$  rays will therefore also be circularly polarized. The process is reversed at the upstream mirror and the FEL photons re-entering the wiggler will have the horizontal polarization optimal for the FEL gain. However, the permanent solution for having a fully controllable and arbitrary polarization entails the installation and use of a new electromagnetic wigglers. A new helical undulator (OK-5) has been constructed by Novosibirsk, Russian. The OK-5 undulator provides both linearly polarized  $\gamma$  rays in both polarization states and circularly polarized light of both helicities. Circularly polarized photons have been demonstrated in the three-body photodisintegration of  ${}^3\text{He}$  at HI $\gamma$ S. New FEL mirrors are on order and operation above 100 MeV range is expected in the next two years.

### A High-Pressure Polarized ${}^3\text{He}$ Gas Target

The polarized  ${}^3\text{He}$  target is based on the principle of spin exchange between optically pumped alkali-metal vapor and noble-gas nuclei[31]. The design is similar to that used in electron scattering experiments in Hall A at Jefferson Lab (JLab) [32]. The polarized  ${}^3\text{He}$  target is centered around an alumino-silicate glass cell that contains 7-10 atmospheres of  ${}^3\text{He}$  gas. The cell is separated into two chambers, one where the gas is polarized and one where the gas interacts with the photon beam. The gas is polarized by spin-exchange with

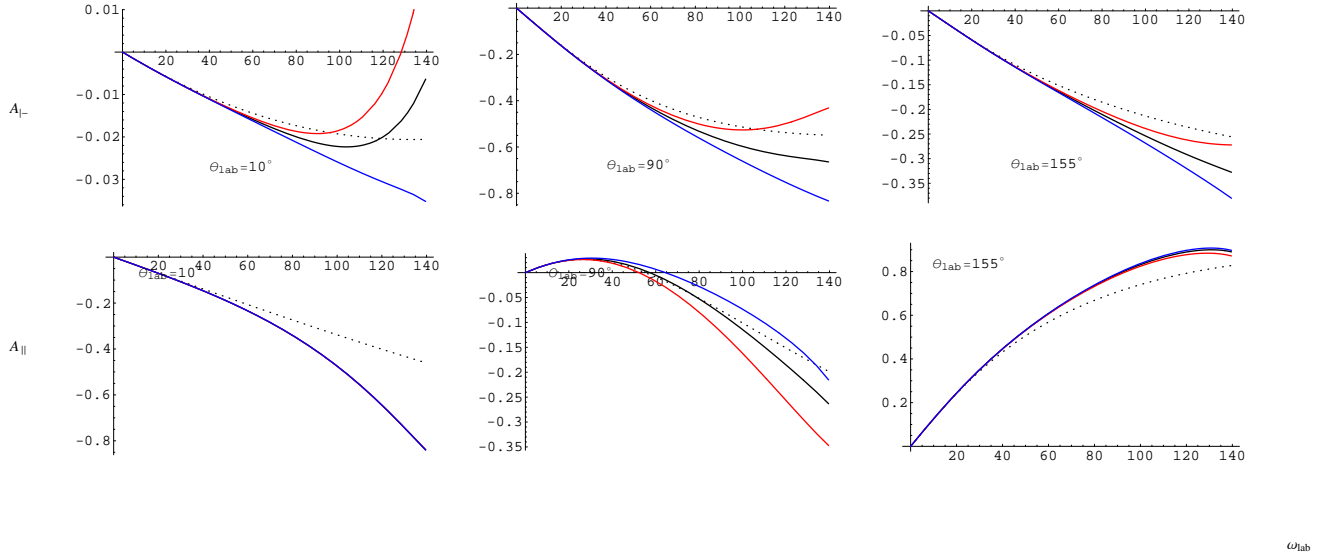
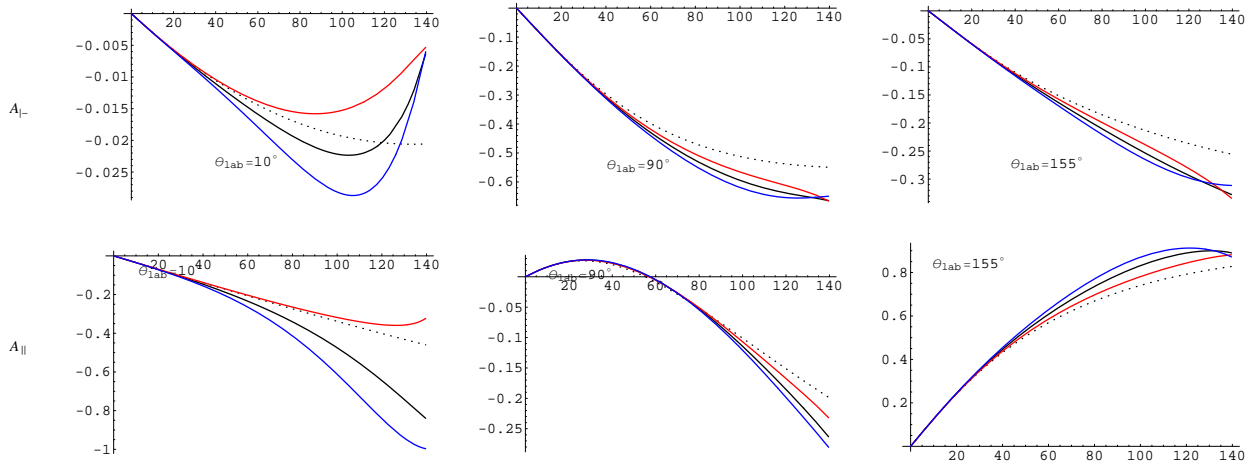


FIG. 8: Compton scattering double polarization asymmetry as a function of photon energy for different photon scattering angle in the lab. The sensitivity to proton spin polarizability  $\gamma_3$  is shown by the difference between red (blue) curve and the black curve (see text for details).

optically polarized rubidium vapor. Rubidium, like all alkali metals, can be polarized by exposing the vapor to circularly polarized laser light at an excitation energy of the valence electrons in a magnetic field. The laser light only excites electrons from one spin substate, forcing all the electrons in the rubidium vapor to accumulate in the opposite spin substate. The  $^3\text{He}$  nuclei is polarized through a hyperfine interaction with the rubidium electrons.

The regular  $^3\text{He}$  cell (Rb only) sits in the middle of a 25 Gauss field generated by a single-layer solenoid. The upper chamber sits in a 170 °C oven which keeps the rubidium as vapor. The laser light is produced by a set of diode lasers and is made circularly polarized by a set of quarter-wave plates. Polarization will be monitored using the NMR technique of adiabatic fast passage (AFP) [33]. The signals are calibrated by comparing the  $^3\text{He}$  NMR signals with those of water. An additional polarization system measuring the electron paramagnetic resonance (EPR) of rubidium is also used as an additional technique to determine the target polarization.

A hybrid approach to polarizing  $^3\text{He}$  atoms, by adding vaporized potassium to the pumping chamber, was first proposed by Happer and co-workers [34]. In this case, the temperature of the upper chamber goes up to 245 °C due to higher K vaporizing temperature. The advantage of this method is as follows: Rb atoms are polarized through the standard optical pumping, they then transfer the angular momentum to potassium atoms. Spin-exchange collisions between  $^3\text{He}$  and K atoms subsequently polarize  $^3\text{He}$  atoms. The likelihood of



$\omega_{\text{lab}}$

FIG. 9: Compton scattering double polarization asymmetry as a function of photon energy for different photon scattering angle in the lab. The sensitivity to proton spin polarizability  $\gamma_4$  is shown by the difference between red (blue) curve and the black curve (see text for details).

rubidium to potassium to  $^3\text{He}$  spin-exchange is significantly higher than that of rubidium to  $^3\text{He}$ ; therefore one would expect the SEOP process for hybrid cells to be more efficient than a Rb-only-cell.

For each target cell, a complete set of tests consists of the following steps: first, use SEOP technique to pump up the cell, after the  $^3\text{He}$  NMR signal saturates, an EPR measurement is conducted so that two independent measurements provide accurate determination of the target polarization. A relaxation measurement will then be performed. The pump-up measurement is the core of the complete test. Our systematic study shows that the laser power, laser spectrum and oven temperature are three major factors that determine the  $^3\text{He}$  NMR signal height for a given  $^3\text{He}$  target. So laser tuning, optics alignment and maintaining a stable oven temperature are essential. The relaxation measurement is carried out by turning off the laser and heater and monitoring the NMR signal as a function of time. The data are taken every 3 hours. To calculate the relaxation time of the cell, the AFP spin flip inefficiency needs to be taken into account. By performing NMR measurements consecutively over a short period of time, the AFP spin flip inefficiency is determined by averaging over 10 measurements. The relaxation time is then determined by fitting the data with an exponential decay function with the AFP spin flip inefficiency as the correction factor.

In total eight  $^3\text{He}$  cells have been tested for the proposed Compton experiment. Two are the Rb-only-cells, and the rest are the hybrid cells (Rb+K), all filled at the college

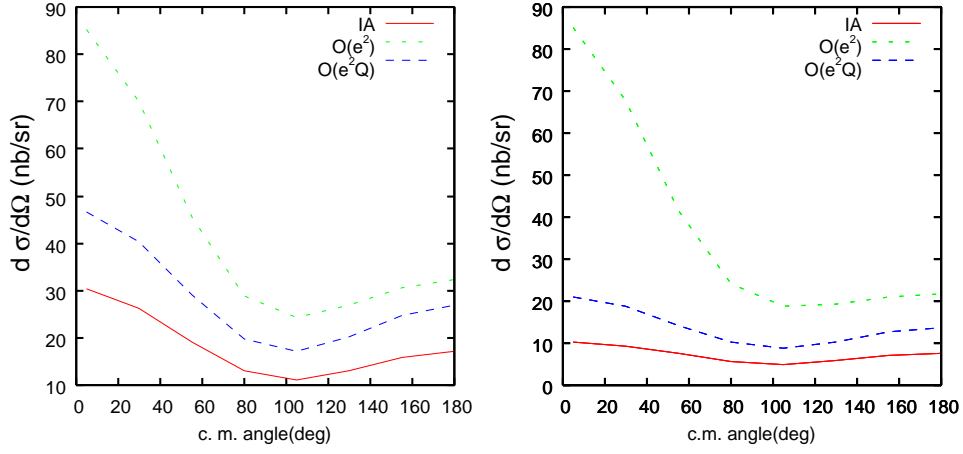


FIG. 10: Calculations of DCS at 100 MeV (left) and 120 MeV (right).

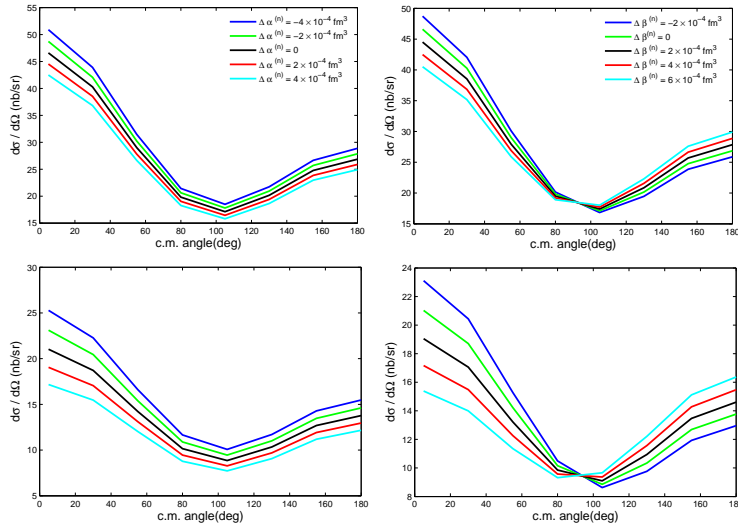


FIG. 11: Calculations of elastic Compton scattering from  $^3\text{He}$  DCS sensitivities to  $\alpha_n$  (left) and  $\beta_n$  (right) for  $\omega = 100$  MeV (upper panel) and 120 MeV (lower panel).

of William and Mary. The names “Kosmo” and “Kelly” are given to the Rb-only-cells, while “Katrine”, “Kramer”, “Jagger”, “Richards”, “Elvis”, “Princeton” and “Bolt” are given to hybrid cells.

The results for the Rb-only-cells are obtained under the following condition: the magnetic holding field is 25 G, the oven operating temperature is 170-175 $^{\circ}\text{C}$ , which is optimal for laser absorption. The experimental condition for hybrid cells is slightly different, and the optimal oven temperature is around 238 $^{\circ}\text{C}$  due to higher K vaporing temperature. For all these measurement, two 60-watts lasers are used. Table I summarizes results for six out of the eight cells. The highest polarization of  $^3\text{He}$  that was achieved of “Bolt” cell is  $\sim 62\%$  at “Bolt” cell [35]. The steady increase of  $^3\text{He}$  polarization can be seen from Fig. 16. For more

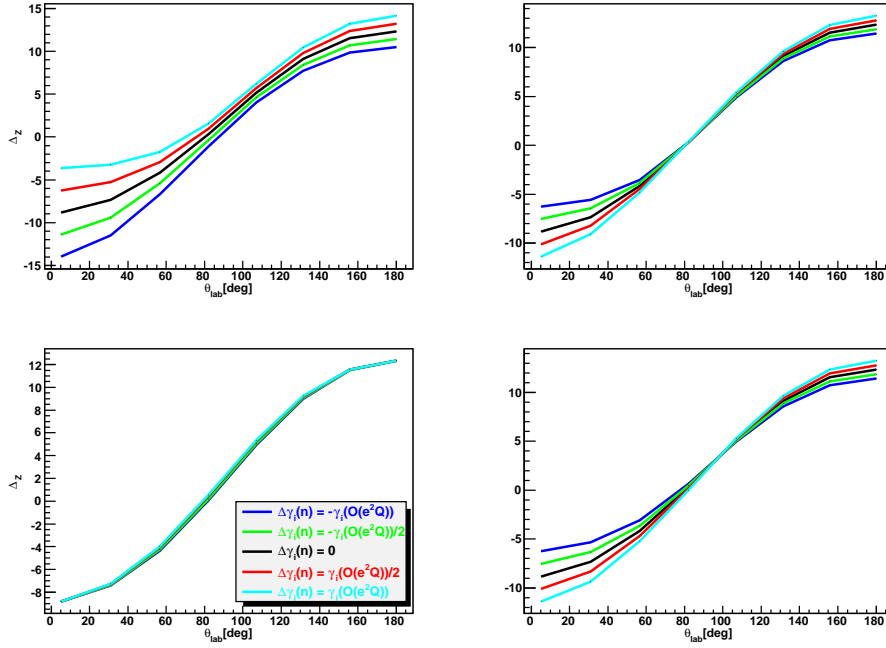


FIG. 12: Sensitivities of  $\Delta_z$  to neutron spin polarizabilities,  $\gamma_i$  at  $\omega=120$  MeV.

Cell	Kosmo	Kelly	Katrine	Elvis	Richards	Bolt
Polarization	34.1%	34.3%	38.5%	46.1%	33.2%	61.6%
EPR Signal(kHz)	37.7	36	37.4	N/A	34	35.2
Lifetime(hrs)	$63.5 \pm 0.3$	$68 \pm 0.4$	$33.2 \pm 0.1$	$36.4 \pm 0.15$	$34 \pm 0.1$	$33.1 \pm 0.04$
Pumpup time(hrs)	$23.5 \pm 0.7$	$16.3 \pm 0.3$	$13.2 \pm 0.4$	$10.8 \pm 0.1$	$7.3 \pm 0.2$	$8.7 \pm 0.12$
EPR Calibration const	0.905	0.951	1.029	1.03	1.001	1.5

TABLE I: Test results for six target cells

details about the target, refer to [36].

The Helmholtz coils can not to be applied for this experiment because of the NaI detectors near the target chamber. A single layer solenoid is therefore developed to provide the holding field with a fractional gradient of  $10^{-3}/\text{cm}$  for  $^3\text{He}$  target system. A COMSOL simulation has been completed for the solenoid. The solenoid, 100 cm long and 18.0 cm in radius, contains the target cell and the oven. It consists of 1 mm copper wire (AWG 18) winding around a hollow cylindrical Mylar support, the the current carried by the wire is around 1 A, as illustrated in Fig. 17. The byproduct is that the scattered photons will loss  $\sim 8\%$  to  $10\%$  events after they pass through the solenoid.

### Target Collimator

The design of the target collimator can be found in Fig. 17. The goal of the target collimator is to shield photons generated from the target windows, which are consider the major

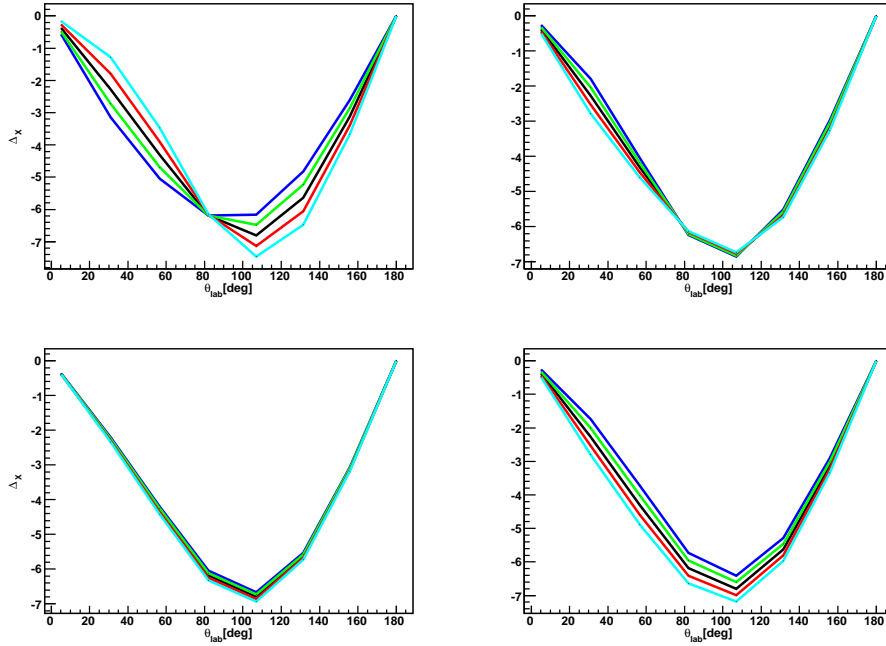


FIG. 13: Sensitivities of  $\Delta_x$  to neutron spin polarizabilities,  $\gamma_i$  at  $\omega=120$  MeV.

background contribution to the elastic Compton scattering peak. The angular acceptance effect for the target collimator is shown in Fig 18.

### The HI $\gamma$ S NaI Detector Array (HINDA)

HI $\gamma$ S can provide photon flux more than  $10^7$ /sec/MeV for Compton scattering experiment. Moreover, even with the high intense photon beams of HI $\gamma$ S, the small cross section in Compton scattering reactions along with the demands for high precision data, make it essential to have a photon detector array which offers high efficiency, good energy resolution and large acceptance.

We propose to utilize the HI $\gamma$ S NaI Detector Array (HINDA) for this Compton scattering experiment. The detection system consists of eight NaI detectors ( $16\frac{1}{4}$  in.  $\times$  12 in. long) with eight PMTs (2 in. in diameter), as illustrated in Fig. 19. All of these detectors consists of a large NaI core ( $10\frac{1}{2}$  in.  $\times$   $10\frac{1}{2}$  in.) surrounded by an active "shield" crystals (NaI(Tl)), which enables rejection of background events as well as an extension of the core to re-sum first-escape events. Borated paraffin is used to reduce neutron events in the core detector. Good shielding for the detector system, especially PMTs is required to ensure the detectors work in a good condition. Since magnetic fields are one of the most important influences on PMTs. It is common practice to shield PMTs with a mu-metal screen which cover around the PMTs' tubes.

These eight NaI detectors are proposed to be allocated at three different angles  $40^\circ$ ,  $60^\circ$  and  $140^\circ$  with respect to the incident photon beam (two detectors at  $40^\circ$ , three at other two angles), and positioned 60 cm away from the target center in order to reach large acceptance. A preliminary design for the HINDA support structure is shown in Fig. 20. This design allows the detectors to be placed in different configurations and used for other

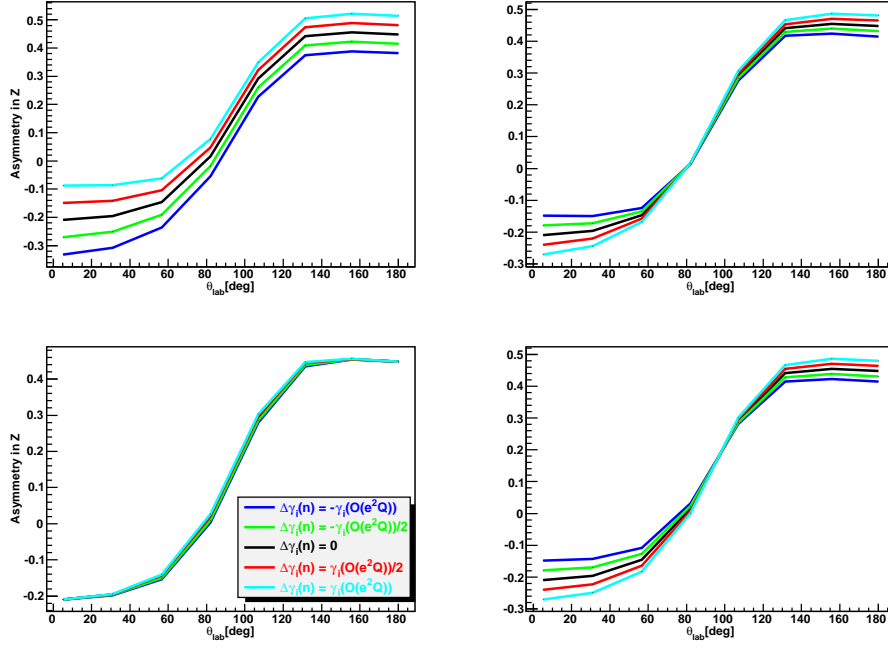


FIG. 14: Sensitivities of  $A_z$  to neutron spin polarizabilities,  $\gamma_i$  at  $\omega=120$  MeV.

experiments.

More recently, the first experimental run with HINDA was performed at HI $\gamma$ S (four NaI detectors were used). The preliminary results show that the NaI detectors worked well with the proper electronics setup [38]. The electronics for each NaI detector have two different setups: CLEAN (anti-coincidence between the shield and the core) and CONIC (coincidence between the shield and the core). CLEAN model can help reduce the background from the environment, while CONIC model is used to isolate the first escape peak from the core. The test result is shown in Fig. 21.

If the gamma-ray peak is summed from one width above the centroid to two widths below, it is found that the efficiency is  $\sim 57\%$  for photon energies between 20 and 120 MeV. The energy resolution of these detectors, has been measured to be 3% at 20 MeV [37], and is expected to be close to 2% at higher energies [37].

In summary, an array with eight fully equipped NaI detectors is ready for the Compton scattering experiment. The HINDA detection system will provide counting rates which will allow us to perform the measurements described in this proposal in the number of hours anticipated for this program.

## Background study

For elastic Compton scattering on  $^3\text{He}$ , the HINDA detection array is used only to detect single photon events. The photon events are binned by scattering angle and then cuts are made on the photon energy to keep the events from quasi-elastic scattering. The quasielastic scattering events are less than 5% of the total number of accepted events.

Since NaI detector does not discriminate neutron and gamma, neutron from three-body photodisintegration of  $^3\text{He}$  is another source contributes to the final background. Calcu-

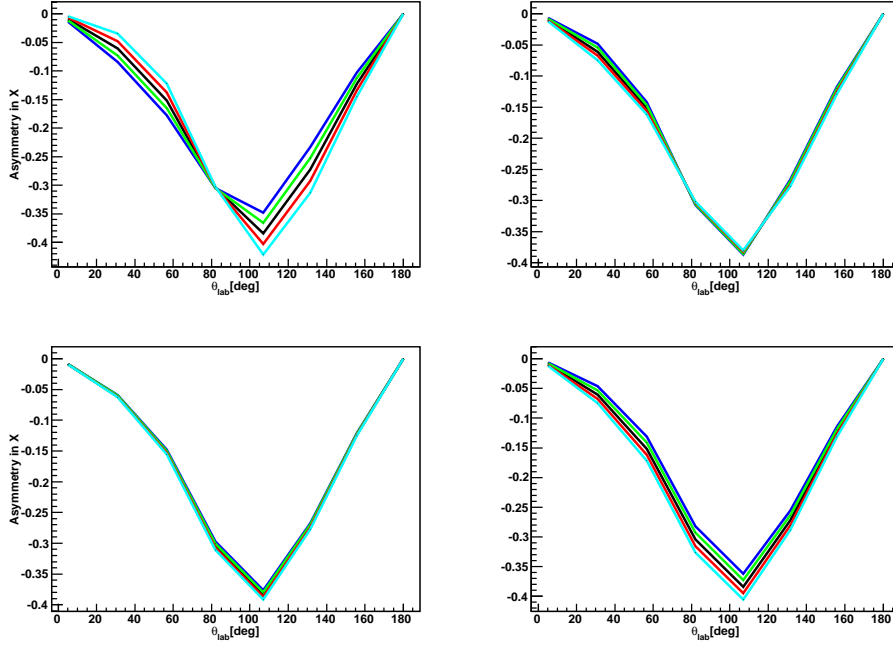


FIG. 15: Sensitivities of  $A_x$  to neutron spin polarizabilities,  $\gamma_i$  at  $\omega=120$  MeV.

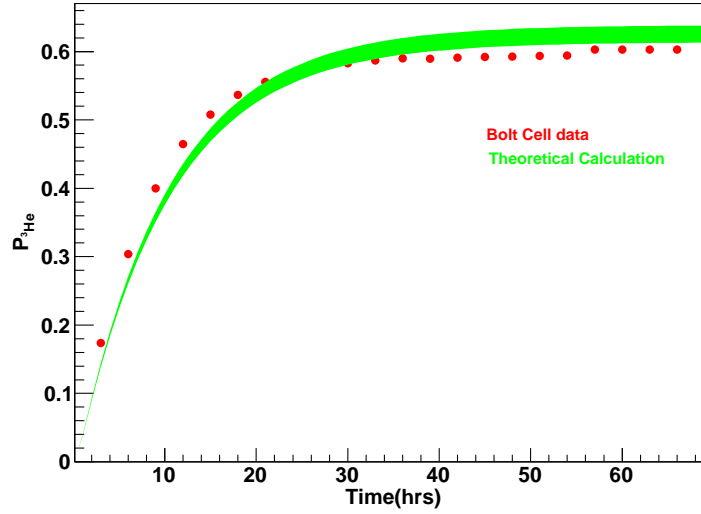


FIG. 16: Polarization of  $^3\text{He}$  with respect to the pumping time. Bolt cell data is in red and theoretical model including uncertainty is in green

lation [39] shows that the maximum kinematics energy of neutron from three-body photo-disintegration of  $^3\text{He}$  can reach is  $\sim 73$  MeV, which does not contribution to the elastic scattering region.

Not only Compton Scattering from the polarized  $^3\text{He}$  contributes to the elastic scattering region, Compton scattering from the target chamber windows and nitrogen gas inside the target also occur. By applying the target collimator, the contributions from the target

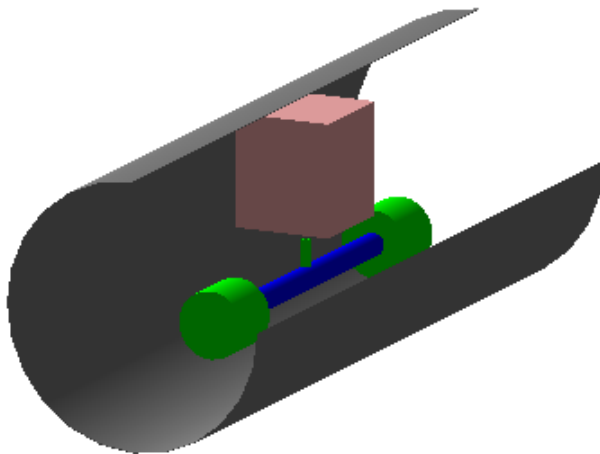


FIG. 17: New target design for proposal experiment. Solenoid (in Gray, one side open for view), Target chamber (in Blue) and Target Collimator (in Green) are also display here.

chamber windows are mostly reduced. In the proposed experiment, a reference target cell filled with nitrogen gas will be used to estimate the background contribution from nitrogen gas.

### Projected Measurements from elastic Compton scattering process

We propose to carry out double polarized elastic Compton scattering measurements from  $^3\text{He}$ . Both the spin-dependent asymmetry and the helicity-dependent differential cross-section difference will be formed from the data. In projecting these results, we used a photon flux of  $5 \times 10^7$  /sec for a 120 MeV photon beam with 3 % energy spread, and a 50% polarized  $^3\text{He}$  target with target thickness of  $1.1 \times 10^{22}$  atoms/cm<sup>2</sup>, list in Table II. The circular polarization of the photon beam is taken to be 100%. Monte Carlo simulations based on the GEANT4 code are completed for this experiment. Physics event generators have been developed to simulate both elastic and quasifree scattering from a polarized  $^3\text{He}$ . The modules of target and HINDA system are implemented in the simulation. Target collimator effect is also included in the simulation. The simulation generates events from  $^3\text{He}$  elastic scattering and tracks the resulting paths of the scattered particles. The NaI detection array then record the scattered photons, and a 60% detection efficiency is used for each NaI detector in the simulation. The event rate was estimated using the GEANT4 simulation of photon scattering from a polarized  $^3\text{He}$  target.

When the target is polarized along the beam direction (parallel or anti-parallel), the longitudinal asymmetry is formed by:

$$A_z = \frac{1}{P_t P_b} \frac{N_{\uparrow\uparrow} - N_{\uparrow\downarrow}}{N_{\uparrow\uparrow} + N_{\uparrow\downarrow}} \quad (24)$$

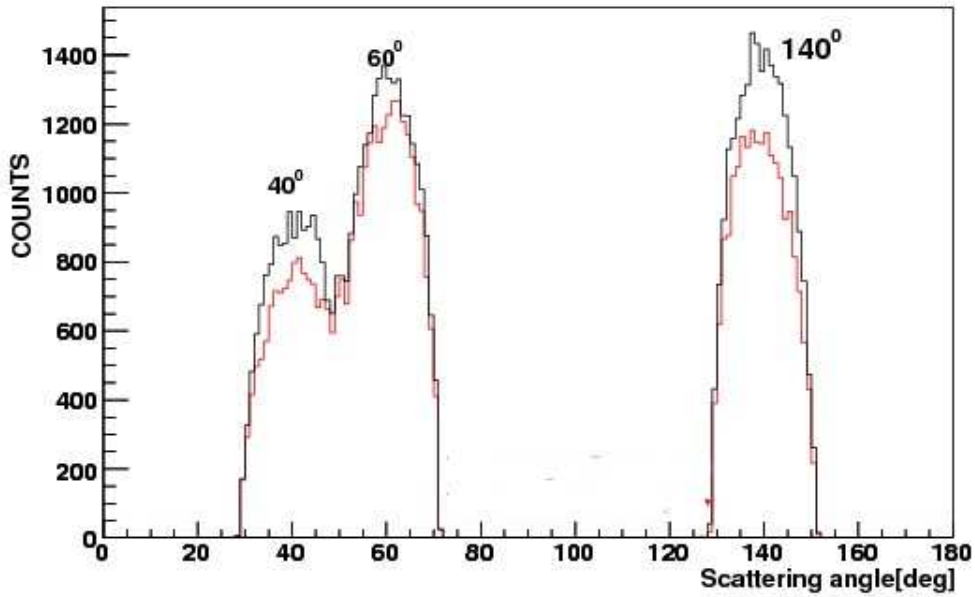


FIG. 18: Angular acceptance effect of the target collimator. The black line shows the acceptance without the collimator and the red line shows the acceptance with the collimator.

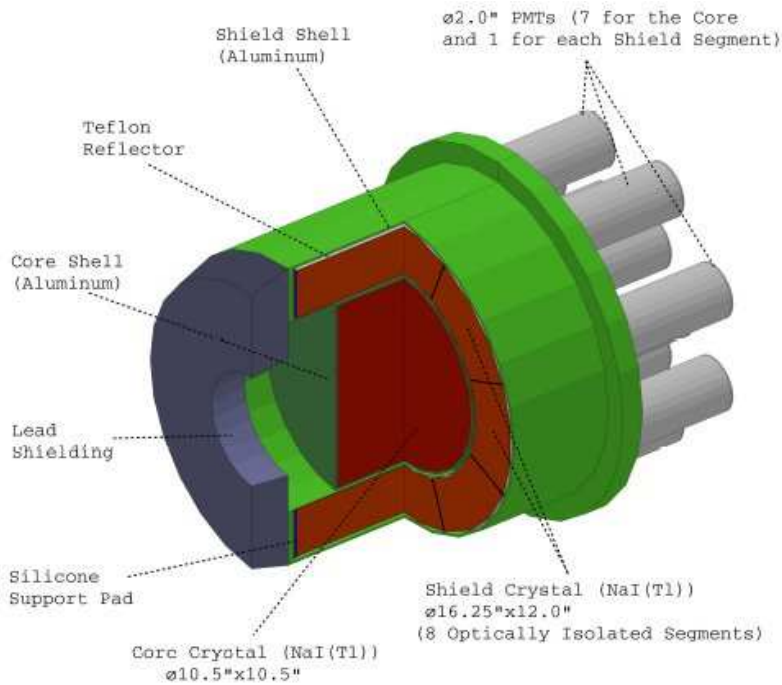


FIG. 19: A NaI detector assembly with the core detector, shielding and front lead collimator

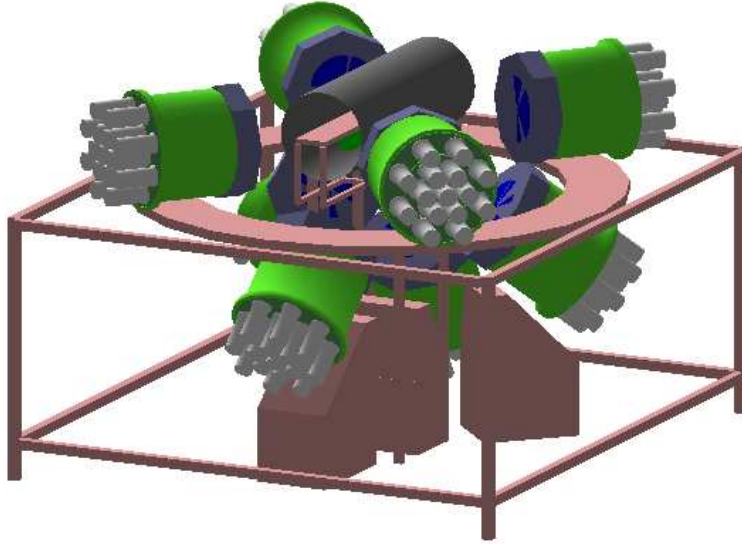


FIG. 20: The proposed experimental setup for Compton scattering

Parameter	Value
Photon Flux	$5 \times 10^7$ photons/s
Photon circular polarization	$\sim 100$ %
Target Density	$1.1 \times 10^{22}$ nuclei/cm <sup>2</sup>
Effective Target Length	40 cm
Target Polarization	$\sim 50$ %
NaI Detection efficiency	0.60

TABLE II: *List of Parameters used for simulation*

where  $N_{\uparrow\uparrow}$  ( $N_{\uparrow\downarrow}$ ) refers to the number of gamma events detected by NaI in the parallel and anti-parallel case.  $P_t$  and  $P_b$  are the target and beam polarization, respectively.

The projected results for  $\Delta_z$  and  $A_z$  are shown in Fig. 22 and Fig. 23, respectively.

### Anticipated results on Neutron Spin Polarizabilities

The nucleon spin polarizabilities have been calculated by several groups [15, 16, 25] at the next-to-leading order (NLO) in chiral perturbation theory. Predictions on all four neutron spin polarizabilities at NLO in heavy-baryon chiral perturbation theory by Kumar, McGovern and Birse [16] are:

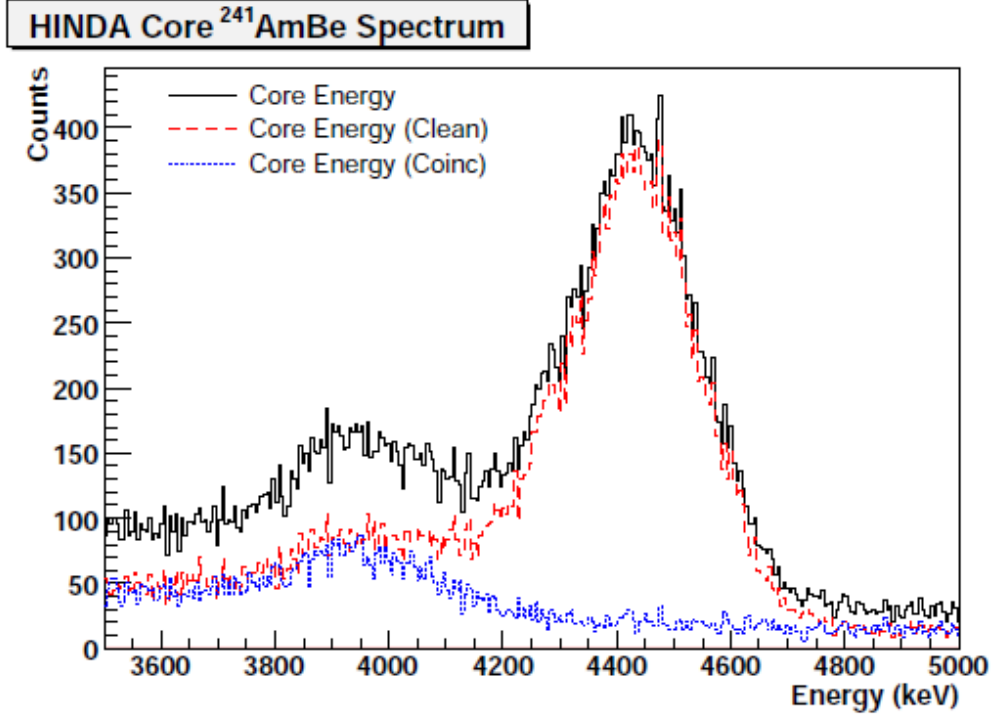


FIG. 21:  $^{241}\text{AmBe}$  spectrum in HINDA

$$\begin{aligned}
 \gamma_1 &= [-21.3]\tau_3 + 4.5 - (2.1 + 1.3\tau_3) \\
 \gamma_2 &= 2.3 - (3.1 + 0.7\tau_3) \\
 \gamma_3 &= [10.7]\tau_3 + 1.1 - (0.8 + 0.1\tau_3) \\
 \gamma_4 &= [-10.7]\tau_3 - 1.1 + (3.9 + 0.5\tau_3) \\
 \gamma_0 &= 4.5 - (6.9 + 1.5\tau_3) \\
 \gamma_\pi &= [-42.7]\tau_3 + 4.5 + (2.7 - 1.1\tau_3),
 \end{aligned} \tag{25}$$

where  $\tau_3 = -1$  for neutron, and the term in brackets are the third-order anomalous contribution. The values of the neutron spin polarizability are  $\gamma_1 = 25.0$ ,  $\gamma_2 = -0.1$ ,  $\gamma_3 = -10.3$ ,  $\gamma_4 = 13.0$ ,  $\gamma_0 = -0.9$ , and  $\gamma_\pi = 51.0$ . One can see that the rather large absolute polarizability values for  $\gamma_1$ ,  $\gamma_3$ ,  $\gamma_4$  and  $\gamma_\pi$  are due to the anomalous contribution. Several authors [14, 24] define the nucleon spin polarizabilities differently from those of Kumar, McGovern and Birse [16] and Ji *et al.* [25] by removing the pion pole contribution. The corresponding neutron spin polarizability values obtained at the NLO in heavy-baryon chiral perturbation theory [16] using the definition of Refs. [14, 24] are therefore:  $\gamma_1 = 3.7$ ,  $\gamma_2 = -0.1$ ,  $\gamma_3 = 0.4$ ,  $\gamma_4 = 2.3$ ,  $\gamma_0 = -0.9$ , and  $\gamma_\pi = 8.3$ .

Combining both the  $A_z$  and the  $\Delta_z$  measurements, the proposed elastic Compton scattering from  $^3\text{He}$  has the following statistical sensitivity to individual neutron spin polarizability  $\frac{\sigma_{\gamma_1}}{\gamma_1}$ ,  $\frac{\sigma_{\gamma_2}}{\gamma_2}$  and  $\frac{\sigma_{\gamma_4}}{\gamma_4}$  are: 16.9%, 19.1% and 20.6%, respectively.

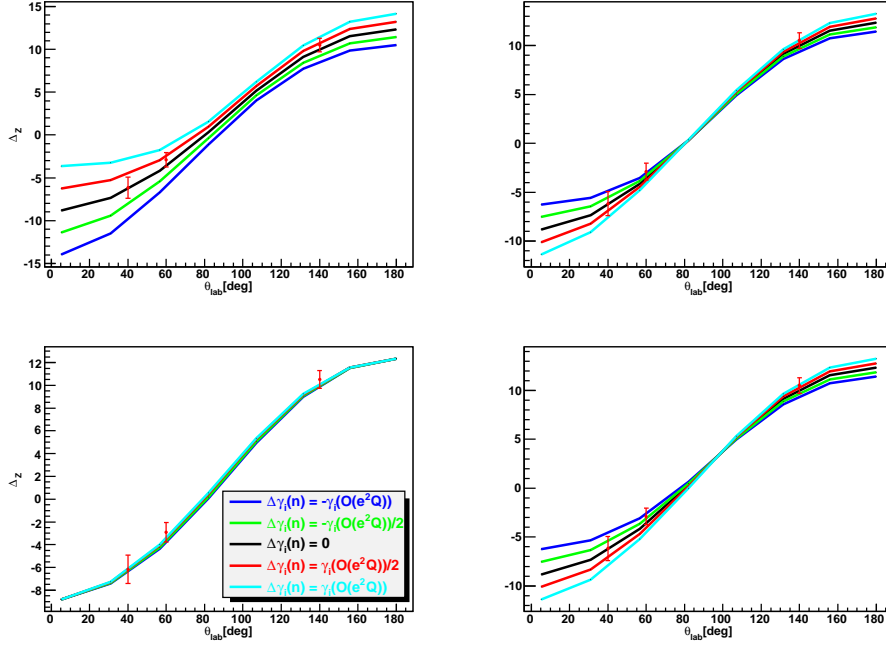


FIG. 22: The projected sensitivity to the neutron spin polarizability  $\gamma_i, i = 1 - 4$  from spin-dependent differential cross section difference measurement from a polarized  $^3\text{He}$  target at HIGs, as a function of photon scattering angle in the laboratory frame. The incident photon beam is circularly polarized at an energy of 120 MeV with a flux of  $5 \times 10^7/\text{sec}$ . The  $^3\text{He}$  target spin is aligned parallel and anti-parallel to the incident photon momentum direction. The running time is 1000 hours with 100% efficiency.

Scattered $\gamma$ Angle	Parallel(counts/hr)	Anti-Parallel(counts/hr)
40°	4.2	6.0
60°	5.8	7.2
140°	7.8	2.9

TABLE III: *Count rates of different scattered angles at incident beam energy 120 MeV*

### Beam time Request

An estimate of event rates are listed in Table III for elastic Compton scattering from polarized  $^3\text{He}$ . We have assumed the photon beam flux of  $5.0 \times 10^7/\text{sec}$ , an effective target length of 40 cm with 10 amgs of  $^3\text{He}$  gas and a target polarization of 50 %. The target collimator effect has been taken into account in the GEANT4 simulation of the acceptance. A 60% detection efficiency was used for the NaI detector in the simulation.

We propose 600 hours of beam time for parallel and anti-parallel configuration, respectively and 60 hours of beam time for nitrogen background measurement. In summary, we request a total of 1260 hours of 100 % efficient photon beam with a minimum photon flux of  $5 \times 10^7/\text{sec}$  with a photon energy spread of 3%.

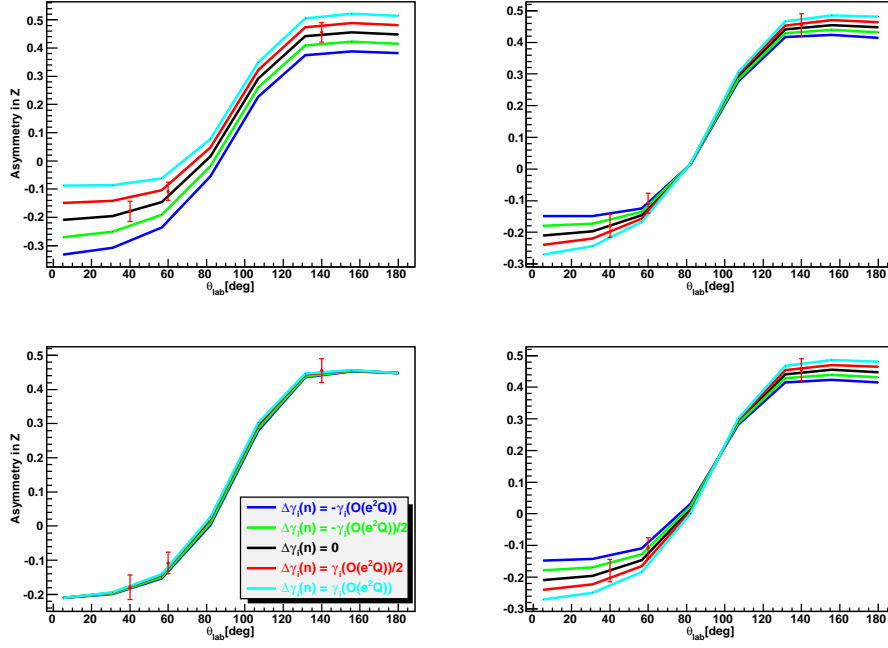


FIG. 23: The projected sensitivity to the neutron spin polarizability  $\gamma_i, i = 1 - 4$  from double polarization asymmetry measurement from a polarized  $^3\text{He}$  target at HIGs, as a function of photon scattering angle in the laboratory frame. The incident photon beam is circularly polarized at an energy of 120 MeV with a flux of  $5 \times 10^7/\text{sec}$ . The  $^3\text{He}$  target spin is aligned parallel and anti-parallel to the incident photon momentum direction. The running time is 1000 hours with 100% efficiency.

## RESPONSIBILITIES

The proposed experiment is a complex, demanding experiment, which requires a circularly polarized photon beam with high intensity ( $5 \times 10^7 / \text{sec}$ ) or higher at the upgraded energy ( $E_\gamma = 120 \text{ MeV}$ ), a high pressure polarized  $^3\text{He}$  gas target with 50 % polarization, and the detection system for the Compton scattered photons. The helicity of the circularly polarized photon beam needs to be flipped faster than on the order of a minute. The photon flux for both helicity needs to be monitored continuously during the experiment better than 2%. The flux monitoring is required for all HI $\gamma$ S experiments. Currently, the photon flux can be determined to a precision of 2 – 3%. The achievement of a precision better than 2% in the flux monitoring before the completion of the planned HI $\gamma$ S energy upgrade is anticipated. In addition to the proposed measurements discussed in this proposal, the fast flipping of the beam helicity is also required for the Gerasimov-Drell-Hearn (GDH) Sum Rule experiments on deuteron and  $^3\text{He}$ .

Several of us (Gao, Kramer) have been engaged in experiments using high pressure polarized  $^3\text{He}$  targets for many years in Hall A at Jefferson Lab. Currently, a high-pressure polarized  $^3\text{He}$  target has been built for the HI $\gamma$ S polarized  $^3\text{He}$  program by Gao's group at Duke in collaboration with the T. Averett's group at college of William & Mary. The main responsibility of the W&M group is in the filling of high pressure  $^3\text{He}$  target cells. The polarized  $^3\text{He}$  target was used for the first experiment at HI $\gamma$ S on three-body photo-disintegration

of  $^3\text{He}$ . The Radiative Capture group at Duke will take on the responsibilities of the photon detection, electronics and data acquisition for the proposed experiment, and these are the areas in which the group has the expertise. The collaboration has the experience and expertise in carrying out the proposed, challenging experiment.

## ACKNOWLEDGEMENT

We thank D. Choudhury, H.W. Griesshammer, T.R. Hemmert, R. Hildebrandt, J.A. McGovern, D.R. Phillips for stimulating discussions. We also thank J. McGovern and R. Hildebrandt for carrying out various calculations at the proposed kinematic settings of this proposal.

- 
- [1] X. Ji, Phys. Rev. Lett. **78**, 610 (1997); Phys. Rev. D **55**, 7114 (1997).
  - [2] A.V. Radyushkin, Phy. Lett. **B380**, 417 (1996); Phys. Lett. **B385**, 333 (1996); Phys. Rev. D **56**, 5524 (1997).
  - [3] V. Olmos de Leon *et al.*, Eur. Phys. J. A **10**, 207 (2001).
  - [4] M. Schumacher, Prog. Part. Nucl. Phys. **55**, 567 (2005).
  - [5] K. Kossert *et al.*, Phys. Rev. Lett. **88**, 162301 (2002).
  - [6] J.A. McGovern, Phys. Rev. C **58**, 1013 (1998), J. McGovern, private communication.
  - [7] R.P. Hildebrandt, H. Griesshammer, and T.R. Hemmert, Euro. Phys. J. **A20**, 329 (2004).
  - [8] B. Pasquini, D. Drechsel, and M. Vanderhaeghen, hep-ph/0705.0282.
  - [9] D. Choudhury, A. Nogga and D. Phillips, Phys. Rev. Lett. **98**, 232303 (2007).
  - [10] J. Tonnison *et al.*, Phys. Rev. Lett. **80**, 4382 (1998).
  - [11] A.I. L'vov and A.M. Nathan, Phys. Rev. C **59**, 1064 (1999).
  - [12] D. Drechsel, G. Krein, and O. Hanstein, Phys. Lett. B **420**, 248 (1998).
  - [13] D. Babusci, G. Giordano, A.I. L'vov, G. Matone, and A.M. Nathan, Phys. Rev. C **58**, 1013 (1998).
  - [14] T.R. Hemmert, B.R. Holstein, J. Kambor, and G. Knöchlein, Phys. Rev. D **57**, 5746 (1998).
  - [15] G.C. Gellas, T.R. Hemmert, and U.-G. Meissner, Phys. Rev. Lett. **85**, 14 (2000).
  - [16] K.B. Vijay Kumar, J.A. McGovern, and M.C. Birse, Phys. Lett. B **479**, 167 (2000).
  - [17] M. Camen *et al.*, Phy. Rev. C **65**, 032202 (2002).
  - [18] F. Wissmann, *Proceeding of the Symposium on the Gerasimov-Drell-Hearn Sum Rule and the Nucleon Spin Structure in the Resonance Region*, p193, Editors: D. Drechsel & L. Tiator, World Scientific, 2000.
  - [19] K. Kossert *et al.*, Eur. Phys. J. **A16**, 259 (2003).
  - [20] M. Gell-Mann, M.L. Goldberger, and W.E. Thirring, Phys. Rev. **95**, 1612 (1954).
  - [21] S.D. Drell and A.C. Hearn, Phys. Rev. Lett. **16**, 908 (1966); S. Gerasimov, Sov. J. Nucl. Phys. **2**, 430 (1966).
  - [22] A.M. Sandorfi, C.S. Whisnant, and M. Khandaker, Phys. Rev. D **50**, R6681 (1994); the Scattering Analysis Interactive Dial-in (SAID) program, available by TELNET to VTINTE, 1993.
  - [23] J. Ahrens *et al.* [GDH Collaboration], Phys. Rev. Lett. **87**, 022003 (2001).
  - [24] D. Drechsel, B. Pasquini and M. Vanderhaeghen, Physics Report **378**, 100 (2003).

- [25] X. Ji, C.-W. Kao, and J. Osborne, Phys. Rev. D **61**, 074003 (2000).
- [26] M.C. Birse, X.D. Ji, and J.A. McGovern, Phys. Rev. Lett. **86**, 3204 (2001).
- [27] B. Blankleider and R.M. Woloshyn, nmPhys. Rev. C **29**, 538 (1984).
- [28] J.L. Friar *et al.*, Phys. Rev. C **42**, 2310 (1990).
- [29] D. Choudhury, private communications.
- [30] B. A. Perdue *et al.*, Phys. Rev. C **70**, 064305 (2004).
- [31] M. A. Bouchiat, T. R. Carver and C. M. Varnum, Phys. Rev. Lett. **5**,373 (1960)  
N. D. Bhaskar, W. Happer, and T. McClelland, Phys. Rev. Lett. **49**, 25 (1982)  
W. Happer *et al.*, Phys. Rev. **A29**, 3092(1984)
- [32] J.S. Jensen, Ph.D. Thesis, California Institute of Technology, 2000 (unpublished), available from  
<http://www.jlab.org/e94010/>;  
P.L. Anthony *et al.*, Phys. Rev. D, **54** 6620 (1996).
- [33] A. Abragam, *Principles of Nuclear Magnetism* (Oxford University Press, New York, 1961).
- [34] W. Happer, G.D.Cates, M.V.Romalis, and C.J.Erickson, U.S.Patent No.6318092 (2001)
- [35] Q.Ye, G.Laskaris Eur.Phys.J.a 44, 55-61(2010).
- [36] K. Kramer *et al.*, Nucl.Instrum.Methods: Phys. Rev. A 582, 318(2007)
- [37] H. R. Weller and N. R. Roberson, Rev. of Mod. Phys., Vol 52, No. 4, 699 (1980); H. R. Weller and N. R. Roberson, IEEE Transactions on Nuclear Science, Vol. NS-28 , 1268, (1980).
- [38] P.P. Martel et al, Nuclear Instrumentation and Methods, TUNL XLVIII 2008-09 pp.137-138.
- [39] R.Skibinski, Jagiellonian University, private communication (2009)
- [40] M.W. Ahmed, G. Feldman, V.N. Litvinenko, S.O. Nelson, B.E. Norum, B. Perdue, I.V. Pinayev, B. Sawatzky, A.P. Tonchev, Y. Wu and H.R. Weller, Nucl. Instrum. Meth. **A510**, 440 (2004).
- [41] J. Chen, X. Ji, and Y. Li, nucl-th/0408003; J. Chen, X. Ji, and Y. Li, nucl-th/0408004.